Understanding Mid-Latitude Jet Variability and Change using Rossby Wave Chromatography: Poleward Shifted Jets in Response to External Forcing

DAVID J. LORENZ *

Center for Climatic Research, University of Wisconsin-Madison, Madison, WI

ABSTRACT

Rossby Wave Chromatography (RWC) is implemented in a linearized barotropic model as a tool to understand the response of the mid-latitude jet to external forcing. Given the background zonal-mean flow and the space-time structure of the baroclinic wave activity source, RWC calculates the space-time structure of the upper tropospheric eddy momentum fluxes. RWC is used to diagnose and understand the poleward shift of the jet in an idealized GCM using the convergence of the vertical EP flux in the upper troposphere as the wave activity source.

The poleward shifted jet is maintained via a selective "reflecting level" on the poleward flank of jet: for a given wavenumber, low phase speed waves are reflected but high phase speed waves are absorbed at the critical level on the poleward flank of jet. When the zonal-mean zonal wind increases on the poleward flank of the jet, a wider range of poleward propagating waves encounter a reflecting level instead of a critical level on the poleward flank. The increased wave reflection leads to increased equatorward propagating waves (and therefore poleward momentum flux) across the jet. Increases in wave phase speeds directly oppose the poleward shift because, in addition to the well-recognized effect of phase speed on wave dissipation in the subtropics, increased phase speeds imply more wave dissipation rather than reflection on the poleward flank via the selective reflecting level.

1. Introduction

This is the second paper of a three part series on the use of Rossby Wave Chromatography (RWC) (Held and Phillips (1987)) to understand the variability of the mid-latitude jet and its response to external forcing. In part I, we describe our implementation of RWC in a linearized non-divergent barotropic model and compare the RWC model to the results from a full General Circulation Model (GCM) (Lorenz (2014a)). In this paper, we describe the mechanisms by which the eddies *maintain* poleward shifted jets in an idealized GCM. In part III, we describe the coupled interaction between the eddy momentum fluxes and the mid-latitude jet and, in particular, why stronger jets shift poleward (Lorenz (2014b)).

The poleward shift of the mid-latitude jet stream and associated storm tracks is one of the most important and robust effects of increasing greenhouse gases (GHG) on the atmospheric circulation. This poleward shift is especially interesting because the direct radiative-convective effects of rising GHG seem to project much more strongly on the strength of the mid-latitude jet. The fact that the jet changes latitude in response to external forcing that either exclusively or predominantly projects on the jet strength has been confirmed by multiple studies with GCMs with simplified physics (Robinson (1997); Haigh et al. (2005); Williams (2006); Chen et al. (2007); Lorenz and DeWeaver (2007); Chen and Zurita-Gotor (2008); Butler et al. (2010); Simpson et al. (2010); Simpson et al. (2012)). The general principle that holds in all these GCM experiments is that forcing which causes mid-latitude jet to get stronger (weaker) also has the additional effect of shifting the jet poleward (equatorward) in latitude (Kidston and Vallis (2012)).

In comprehensive climate models, the jet increases in strength due to increases in the vertically integrated pole-to-equatorward temperature gradient. Two direct

* *Corresponding author address:* David J. Lorenz, Center for Climatic Research, University of Wisconsin-Madison, 1225 W. Dayton St., Madison, WI 53706.
E-mail: dlorenz@wisc.edu

radiative-convective effects of GHG that cause the pole-to-equator temperature gradient to increase are: 1) the tropical troposphere warms more than the extratropics because of the lapse rate constraint imposed by moist convection (Held (1993)) and 2) the troposphere warms while the stratosphere cools (Manabe and Wetherald (1967); Manabe and Wetherald (1980)), which increases the pole-to-equator temperature gradient because the tropopause slopes downward toward the pole (Held (1993); Lorenz and DeWeaver (2007)). Poleward amplification of global warming, which causes an equatorward shift of the jet (Butler et al. (2010)), is a relatively shallow surface phenomena, which is also restricted to the cool season, so it has less effect on the vertically integrated temperature gradient.

There have been many proposed and plausible mechanisms for the sensitivity of jet latitude to jet strength. Due to the dominant role of the eddies on the circulation of the mid-latitudes, all mechanisms involve the interaction between the waves and the mean flow. Chen et al. (2007) propose that increases in jet speed cause wave phase speeds to increase, which then causes the critical levels on the jet flanks to move toward the jet center. Because equatorward wave propagation dominates on a sphere, the primary effect of increasing eddy phase speeds is the migration of the equator-side critical level and its associated eddy-induced negative zonal wind forcing poleward. The relative decrease of winds on the equatorward flank compared to the jet center will then cause further poleward migration of the critical level. If the onset of barotropic instability is important in setting the jet scale (Kidston and Vallis (2010)), then the narrower jet that results directly from the above critical level dynamics is not sustainable and it seems plausible that the jet might broaden towards the poleward flank leading to a poleward shift. Chen et al. (2007) also argue that a positive baroclinic feedback (Robinson (2000)) is important.

Kidston et al. (2011) propose that a robust increase in eddy length scales due to GHG (Kidston et al. (2010)), leads to slower wave phase speeds relative to the background zonal wind. Slower wave phase speeds relative to the mean flow discourage wave breaking and therefore encourage more wave propagation out of the jet (Pierrehumbert and Swanson (1995); Kidston et al. (2011)). Kidston et al. (2011) argue that this effect has the most leverage on the poleward flank of the jet where the critical level is especially close to the latitude of the wave sources. Increasing the source of wave activity on the poleward flank implies positive zonal wind forcing there, leading to a poleward shift. At first sight it may seem that the Chen et al. (2007) and Kidston et al. (2011) mechanisms are incompatible since one mechanism requires increases in phase speed while the other involves decreases. However, since they involve changes in phase speed relative to winds at different locations, they can both operate if winds increase *more* than phase speeds in wave source regions and if winds increase *less* than phase speeds in wave breaking regions (Kidston et al. (2011)). Rivière (2011) also implicate an increase in the eddy length scale on the poleward shift of the jet. However, he argues that the increase in eddy length scale is important because it favors anticyclonic rather than cyclonic breaking of baroclinic waves. On the other hand, the realistic simulations with a linearized barotropic model in Lorenz (2014a), where nonlinear eddy-eddy interactions are parameterized with a uniform and constant diffusion on vorticity, suggest that the details of the wave breaking morphology are not essential for the poleward shift. Also, while Kidston et al. (2011) and Rivière (2011) argue that increases in eddy scale cause the poleward shift, Barnes and Hartmann (2011) suggest that the poleward shift itself causes the increase in eddy length scale, not vice versa. In Lorenz (2014a), we find that changes in eddy length scale are essentially zero when the zonal-mean component of friction is reduced yet the jet still shifts poleward. Nevertheless, the changes in absolute vorticity gradient, β^* ($= a^{-1}\partial_\phi(f + \bar{\zeta})$), are in the correct to sense to decrease phase speeds relative to the wind, and this may act to shift the jet poleward by a similar mechanism as in Kidston et al. (2011).

Kidston and Vallis (2012) propose that stronger jets on a sphere preferentially decrease β^* on the poleward flank of the jet. This increases the range of eddy phase speeds that encounter a turning (reflecting) latitude when propagating toward the poleward flank of the jet. The resulting increase in equatorward propagating waves (from reflected poleward propagating waves), increases the poleward momentum fluxes across the jet and shifts the jet poleward. Kidston and Vallis (2012) argue further that β^* might even change sign on the poleward flank leading to the over-reflection of wave activity. Other studies have also suggested that index of refraction changes are important (Simpson et al. (2009); Simpson et al. (2012); Wu et al. (2013)), however, their views on the specific dynamical mechanisms are different than that of Kidston

and Vallis (2012).

With so many proposed and plausible mechanisms, a way to determine which mechanisms are important and which are not is a top priority. Constructing simpler models on a model hierarchy (Held (2005)) is logical way forward and randomly forced barotropic models have been used for this already (Chen et al. (2007); Kidston and Vallis (2012)). Forced barotropic models are motivated by baroclinic wave life cycle experiments that suggest that eddy life cycles can be usefully partitioned into several distinct stages (Simmons and Hoskins (1978); Hoskins et al. (1985); Held and Hoskins (1985); Thorncroft et al. (1993)). The forced barotropic model is meant to isolate the stage associated with the meridional propagation of wave activity from the stage associated with the generation of wave activity from baroclinic instability, which in this case is parameterized by random forcing. Unfortunately, this approach has been used twice and yielded two separate proposed mechanisms for the poleward shift: 1) increases in phase speed are essential (Chen et al. (2007)), and 2) wave reflection on the poleward flank of the jet is essential (Kidston and Vallis (2012)). Furthermore, Kidston et al. (2011) considered barotropic initial value problems and proposed a third mechanism: changes in wave scale and the associated decreases in phase speed are essential.

We believe the source of the contradictory conclusions involves the forcing of the barotropic models used in the literature so far. All barotropic models used for understanding zonal wind variability and change prescribe a random forcing *directly* to either the vorticity equation (Vallis et al. (2004); Barnes et al. (2010); Barnes and Hartmann (2011); Kidston and Vallis (2012)) or the divergence equation (Chen et al. (2007)). In this paper, on the other hand, we prescribe the baroclinic wave activity source and then determine the forcing, vorticity and all other fields from the wave source under the assumption that the forcing and vorticity are related by the linearized barotropic vorticity equation (Lorenz (2014a)). The model is applied separately to each desired zonal wavenumber and phase speed. Our model (Lorenz (2014a)) essentially implements Rossby Wave Chromatography (RWC) as described by Held and Hoskins (1985); Held and Phillips (1987); Randel and Held (1991): given the background flow and the space-time structure of the baroclinic wave activity source, we calculate the space-time structure of the eddy momentum flux. Some advantages of this technique are: 1) the model can be compared directly to a GCM or to observations using the convergence of the vertical EP flux (Edmon et al. (1980)) in the upper troposphere as the wave source, 2) prescribing the observed wave activity sources eliminates almost all choices regarding the space-time structure of the forcing, 3) the wave activity source is more closely related to the momentum fluxes (i.e. the meridional wave activity flux) that force the zonal-mean zonal wind than the vorticity forcing, and 4) the full space-time structure of the wave activity source and the background flow are decoupled so that one can be changed without impacting the other.

DelSole (2001) also specified the magnitude of the wave activity source at each latitude in a linearized barotropic model. The temporal structure of the forcing, however, was assumed to be white noise, so the space-time structure of the wave activity source is not necessarily realistic. More importantly, specifying the temporal structure makes it impossible to change the phase speed of the waves independently of changes in the background zonal wind. In our approach, on the other hand, the entire phase speed-latitude-wavenumber structure of the wave activity source is specified and can be manipulated to better understand the dynamics.

We find that the RWC model best simulates the GCM momentum fluxes when the non-divergent barotropic vorticity equation is used together with the absolute vorticity gradients from the GCM. Using upper troposphere potential vorticity (PV) gradients (which are everywhere considerably larger than absolute vorticity gradients due to the stretching term) in the RWC model, on the other hand, produces poor mean states where the poleward wave activity flux approaches the strength of the equatorward wave activity fluxes. The fact that the barotropic vorticity equation provides a better simulation suggests that the waves are better viewed as vertical modes, in particular external Rossby waves (Held et al. (1985)). While it makes sense that low phase speed waves behave like external Rossby waves it is not clear why waves with phase speeds between the upper and lower tropospheric $\bar{u}$ are also better simulated using the barotropic vorticity equation. For example, according to the linearized two level model, the propagating waves approaching an upper tropospheric critical level feel the upper level PV gradients (Saravanan (1993)). These issues are the subject of current research.

In this paper, we use RWC to understand the mechanisms that maintain poleward shifted jets in response to

Table 1: Perturbed GCM experiments.

Name	Description	Control Value	Perturbed Value
ZFRIC	decrease friction on zonal mean u	$k_f = 1$ day^{-1}	$k_f = 0.8$ day^{-1} on zonal mean u
TSTRAT	decrease stratosphere temp.	$T_{strat} = 200$ K	$T_{strat} = 195$ K
ΔT_y	increase pole-to-equator temp. diff.	$\Delta T_y = 60$ K	$\Delta T_y = 70$ K
$\Delta\theta_z$TROP	increase tropical static stability	$\Delta\theta_z = 10$ K	$\Delta\theta_z = 13$ K
RAD	decrease thermal relaxation time scale	$k_a = 1/40$ day^{-1} and $k_s = 1/4$ day^{-1}	$k_a = 1/35$ day^{-1} and $k_s = 1/3.5$ day^{-1}
FRIC	decrease friction	$k_f = 1$ day^{-1}	$k_f = 0.8$ day^{-1}

external forcing. The GCM experiments we analyze are exactly the same as those described in Lorenz (2014a). In a companion paper (Lorenz (2014b)), we explore the eddy-zonal flow feedbacks that cause stronger jets to shift poleward. In section 2, we briefly describe the GCM experiments and the implementation of RWC in a linearized barotropic model. Next we explore the general mechanisms responsible for maintaining the poleward shifted jet (section 3). We then present a more detailed, mechanistic view of the dynamics with an emphasis on wave reflection (section 4) and the effect of wave phase speeds on eddy momentum fluxes (section 5). We end with a discussion and conclusions.

2. GCM experiments and RWC model

The dynamical core of the GCM is described in Lorenz (2014a) and all details regarding resolution and integration length can be found there. The standard idealized forcing given in Held and Suarez (1994) is used for the control run. The latitude of the climatological jet in the control run is 42°. To understand the response to external forcing we perturb the parameters of the control run as in Lorenz (2014a) (Table 1). All of the applied perturbations have the direct effect of increasing the strength of the jet and therefore, consistent with the discussion above, they also shift the jet poleward (see Fig. 1 in Lorenz (2014a)). The focus of this paper is on diagnosing and understanding the RWC momentum flux response to $\bar{u}$ and wave activity source spectra from the GCM.

Our implementation of RWC prescribes the covariance between the vorticity and the vorticity forcing for each wavenumber and phase speed under the assumption that the vorticity is related to the forcing by the linearized barotropic vorticity equation on a sphere (see Lorenz (2014a)). The background zonal wind and absolute vorticity field for the barotropic model are weighted vertical averages of the corresponding GCM fields (see Lorenz (2014a)). RWC calculates the eddy momentum flux phase speed spectrum from the background zonal-mean zonal wind, $\bar{u}$, and wave activity source spectrum. The wave activity source spectrum is defined as the convergence of the vertical EP flux (Edmon et al. (1980)) averaged from $\sigma = 0.125$ to $\sigma = 0.525$. The eddy momentum fluxes calculated from RWC are intended to simulate the GCM eddy momentum fluxes averaged over the same σ-level range. The RWC response is defined as the change in eddy momentum fluxes from the RWC simulation with perturbed $\bar{u}$ and wave activity source spectrum minus the RWC simulation with control inputs.

The angular phase-speed spectra (e.g. Randel and Held (1991)) are calculated as in Lorenz (2014a). For all figures in this paper, angular phase speed is given in terms of velocity at 45° latitude in m s^{-1}. In other words, our angular phase speed (c) is related to the angular phase speed in rad s^{-1} (c_ω) by $c = c_\omega a \cos(45°)$, where a is the radius of the earth. The resolution in phase speed for all analysis and figures is 2 m s^{-1}.

A comparison of the RWC momentum fluxes, $\overline{u'v'}$, with the GCM after integrating over all wavenumbers and phase speeds is shown in Fig. 1a. The largest errors are poleward of 50° where the RWC $\overline{u'v'}$ is greater than the GCM. In addition the main positive center of $\overline{u'v'}$ is shifted slightly poleward in the RWC model. The latitude/phase speed spectrum of the wave activity source, which is specified in RWC, peaks on the equatorward flank of the jet but decays much more quickly to zero on the equator side than on the pole side of the jet (Fig. 1b). The latitude/phase speed spectrum of $\overline{u'v'}$ in the GCM shows that poleward (equatorward) momentum (wave activity) fluxes dominate–this is a fundamental asymmetry caused by the spherical geometry. The momentum fluxes are weighted more toward lower phase speeds compared

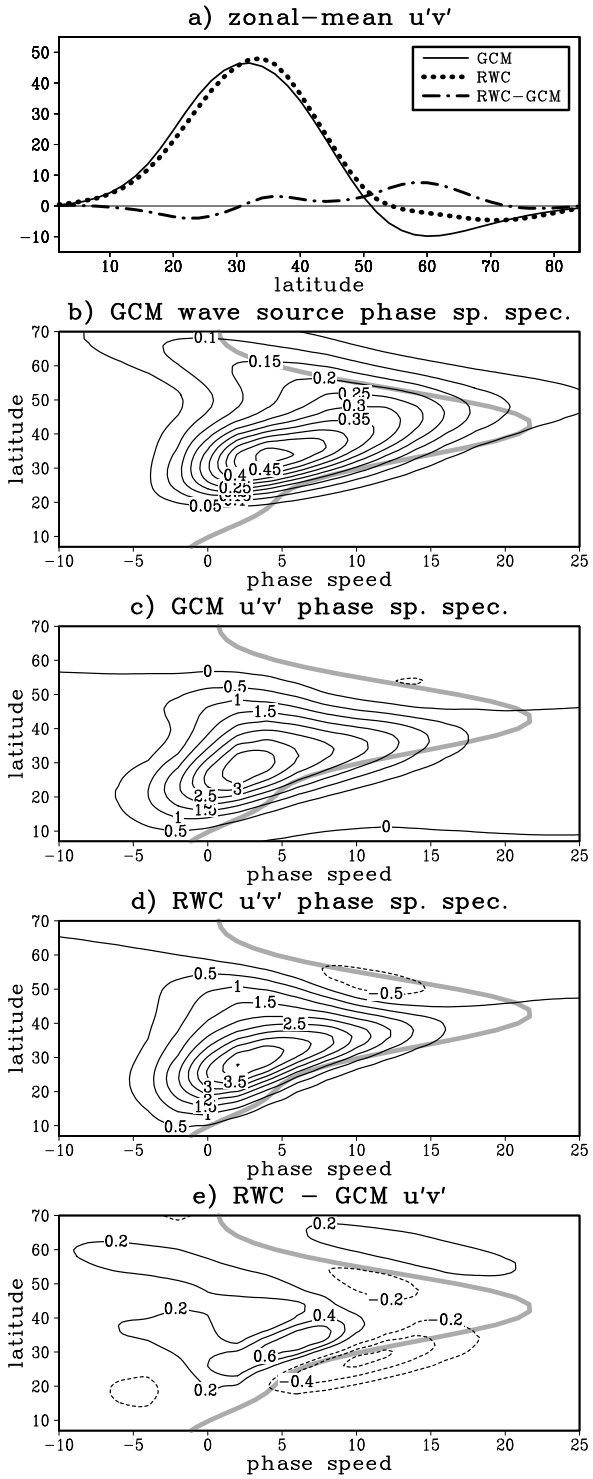

Figure 1: a) RWC eddy momentum flux (dotted), zonal-mean eddy momentum flux averaged from $\sigma = 0.125$ to 0.525 in the GCM (solid) and their difference ($m^2\ s^{-2}$). b) Latitude/phase speed spectrum of the vertical component of EP flux averaged from $\sigma = 0.125$ to 0.525 in the GCM (day^{-1}). The gray line is the critical level. The x-axis is angular phase speed in $m\ s^{-1}$ at 45° (see section 2). c) Latitude/phase speed spectrum of the eddy momentum flux averaged from $\sigma = 0.125$ to 0.525 in the GCM ($m\ s^{-1}$). d) Latitude/phase speed spectrum of the eddy momentum flux from RWC ($m\ s^{-1}$). e) Difference of panels (d) and (c).

to the wave source. The RWC $\overline{u'v'}$ reproduces the general features in the GCM $\overline{u'v'}$ but the distribution in latitude and phase speed tends to be less broad than the GCM (Figs. 1de). In particular, the waves in the RWC model do not propagate as far toward the critical level (gray line) compared to the GCM.[1] Poleward of 45°, on the other hand, the bias in the RWC phase speed spectra might be best described as too much propagation: both equatorward by the slower waves (positive $\overline{u'v'}$) and poleward by the faster waves (negative $\overline{u'v'}$). The fact that the former are overestimated more leads to the biases poleward of 50° in Fig. 1a.

The change in the total $\overline{u'v'}$ (i.e. integrated over wavenumber and phase speed) for each of the six GCM experiments is compared with RWC in Fig. 2. RWC correctly simulates the variability in general structure (monopole versus weak dipole) and the variability in amplitude among the six experiments. In general, the RWC model simulation is too narrow and the nodal line is too far poleward when the $\overline{u'v'}$ changes are of the dipole type. Interestingly, when the RWC model is coupled to $\bar{u}$ these biases are reduced (Fig. 2a) (see Lorenz (2014a)). The RWC model also tends to under-estimate the magnitude of the $\overline{u'v'}$ changes.

While there are clearly significant biases in the RWC model, the RWC simulation reproduces all the general features of the GCM. This suggests that the mechanisms operating in the RWC model are likely the same mechanisms operating in the GCM. Similarly, the mechanisms that do not operate in the RWC probably do not operate in a significant way in the GCM. For more comparisons between the RWC model and the GCM see Lorenz (2014a).

3. General Mechanisms

In this section, we separate the general mechanisms that are associated with the RWC response to the background flow and wave source changes of the GCM experiments described in Lorenz (2014a). By applying the background flow and source changes separately, we can isolate the momentum flux response into the contributions of 1) changes in the phase speed of the wave source, 2) changes in the magnitude of the wave source and 3) changes in the Index Of Refraction (IOR) associated with the background flow. Given the wave source phase speed

[1] Note that the linear RWC model has non-zero momentum flux equatorward of the subtropical critical level. This is due to the strong diffusion in the linear barotropic model (see Lorenz (2014a)).

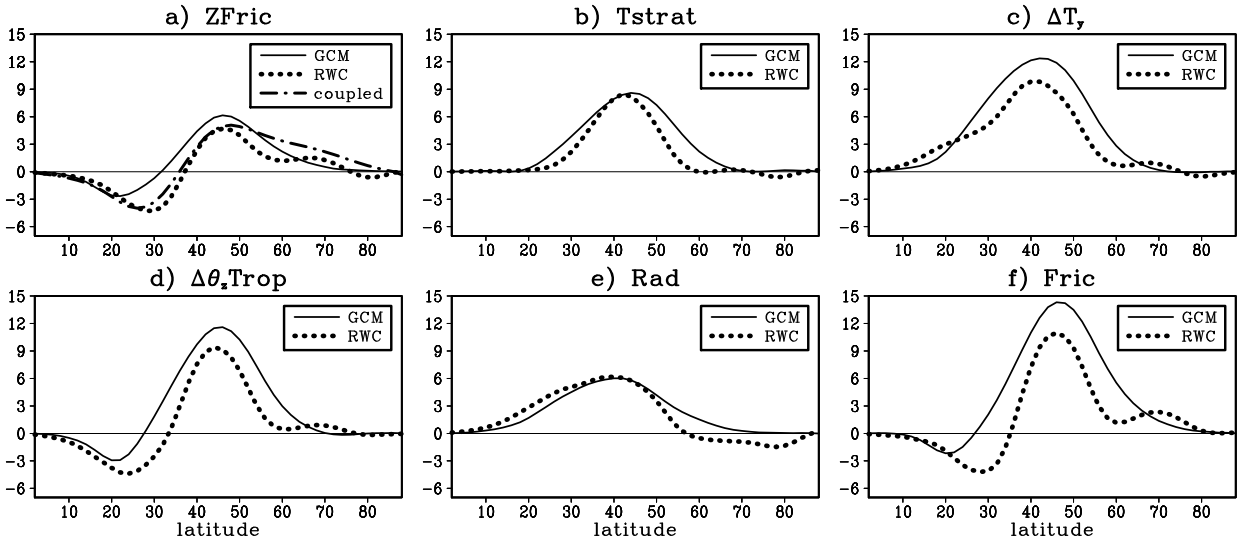

Figure 2: a) The change in zonal-mean eddy momentum flux for ZFRIC in the GCM (solid), RWC (dotted), and for RWC coupled to $\bar{u}$ (m^2 s^{-2}). b) The change in zonal-mean eddy momentum flux for TSTRAT in the GCM (solid) and RWC (dotted) (m^2 s^{-2}). c) As in (b) but for ΔT_y. d) As in (b) but for $\Delta\theta_z$TROP. e) As in (b) but for RAD. f) As in (b) but for FRIC.

spectrum at a given zonal wavenumber and latitude for both the control run, $S_1(c)$, and the perturbed run, $S_2(c)$, the new source associated with phase speed changes is defined as

$$S_{\text{phase}} = S_2(c)\frac{\int S_1(c)dc}{\int S_2(c)dc}. \tag{1}$$

Note that S is constrained to be nonnegative in the RWC model (Lorenz (2014a)), therefore S is set to zero when S is negative.[2] S_{phase} has the same structure as the new wave source, S_2, but is scaled so there is no net change in magnitude. We call this the phase speed term because shifts of the spectrum in c dominate the changes.[3] The new source associated with changes in source magnitude is defined as

$$S_{\text{mag}} = S_1(c)\frac{\int S_2(c)dc}{\int S_1(c)dc}, \tag{2}$$

which has the same structure as $S_1(c)$ but is scaled by an amplitude factor. We also consider the total effect (from both magnitude and phase) of wave source changes on the momentum fluxes. The response to changes in background flow with constant wave source is called the change from IOR because the inviscid, unforced version of the linearized barotropic vorticity equation (see (3) in Lorenz (2014a)) can be written as

$$\cos\phi\frac{d}{d\phi}\left(\cos\phi\frac{d\psi}{d\phi}\right) + l^2\psi = 0, \tag{3}$$

where ψ is the complex streamfunction amplitude for a given phase speed and zonal wavenumber, ϕ is the latitude, and l^2 is the index of refraction:

$$l^2 = \frac{\beta^* a\cos\phi}{\bar{u}/(a\cos\phi) - c_\omega} - m^2, \tag{4}$$

where β^* is the absolute vorticity gradient ($= a^{-1}\partial_\phi(f + \bar{\zeta})$ where f is the Coriolis parameter and ζ is the relative vorticity), and m is the *integer* zonal wavenumber.

In Fig. 3a, we show the contributions of IOR and total wave source changes to the total $\overline{u'v'}$ predicted by RWC for the ZFRIC run as well as the sum of IOR and wave source contribution to gauge the degree of nonlinearity. The positive $\overline{u'v'}$ come from IOR changes and the negative $\overline{u'v'}$ come from wave source changes. The momentum flux convergence ($= \overline{\zeta'v'} = -\cos^{-2}\phi\partial_\phi(\overline{u'v'}\cos^2\phi)$) associated with Fig. 3 are shown in Fig. 4. The $\overline{\zeta'v'}$ from IOR accelerate the flow on the poleward flank of the mean jet (located at 42°) and are responsible for maintaining the poleward shifted jet while the wave source changes oppose the shift (Fig. 4a). Decomposing the source changes into the contributions of the phase speed changes and the magnitude changes we see that the phase

[2] S is dominated by its positive values so this is of little consequence.

[3] For example, in the ZRIC run, the spatial correlation (over c) between S_{phase} and $-dS_1/dc$ is greater than or equal to 0.88 for all latitudes between 30° and 70°. Near 40° the correlation exceeds 0.98.

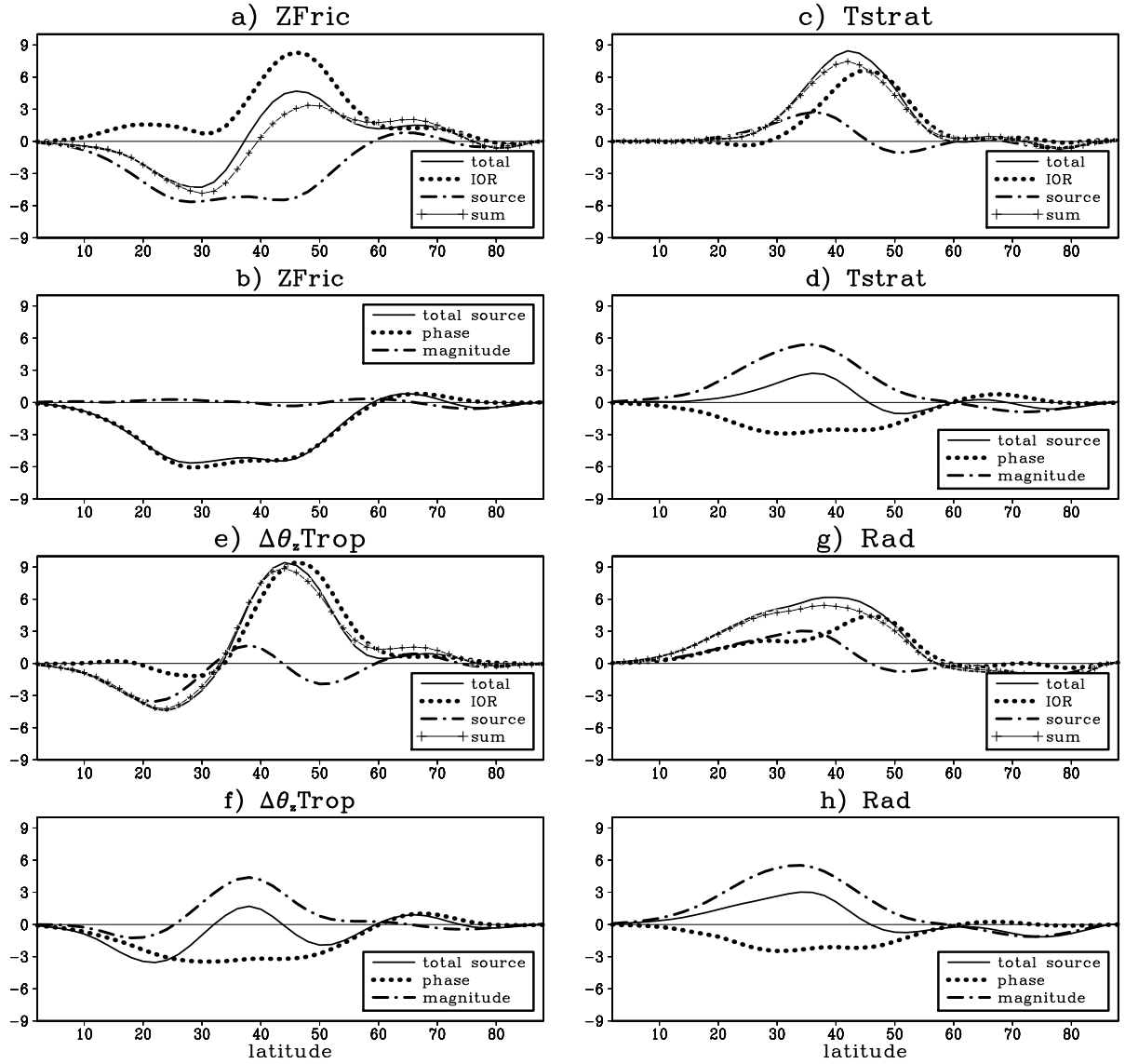

Figure 3: a) The change in eddy momentum flux in RWC for ZFRIC: total change (solid), portion due to changes in IOR (dotted), portion due to changes in wave sources (dash-dotted) and the sum of the IOR and wave source portions (solid with plus signs) ($m^2\ s^{-2}$). b) The change in eddy momentum flux in the RWC model for ZFRIC: portion due to all wave source changes (solid), portion due to changes in the phase speed of the wave sources (dotted) and the portion due to changes in source magnitude (dash-dotted) ($m^2\ s^{-2}$). c) As in (a) but for TSTRAT. d) As in (b) but for TSTRAT. e) As in (a) but for $\Delta\theta_z$TROP. f) As in (b) but for $\Delta\theta_z$TROP. g) As in (a) but for RAD. h) As in (b) but for RAD.

speed changes dominate in this case (Figs. 3b and 4b). We do not show the sum of phase and magnitude changes in this figure because it is nearly identical to the total source contribution. The remaining panels in Figs. 3 and 4 are the same as Figs. 3ab and 4ab but for the runs TSTRAT, $\Delta\theta_z$TROP and RAD. The main difference with the ZFRIC case is the importance of changes in source magnitude. Wave sources get stronger in these simulations because we increase the forcing of the pole-to-equator temperature gradient in some way. Unsurprisingly, these changes tend to strengthen the jet in its current location although there is a very small poleward bias in the TSTRAT and $\Delta\theta_z$TROP case ($\overline{\zeta' v'}$ peaks at 44° while the mean jet is at 42° (Fig. 4)). In summary, the IOR acts to shift the jet poleward, the source phase speeds act to weaken the poleward shift and the source magnitude acts to strengthen the jet in some cases. When RWC is coupled to $\bar{u}$ in experiments analogous to ZFRIC, we see that the RWC model predicts that stronger jets shift poleward (see Lorenz (2014a)). Moreover, when these

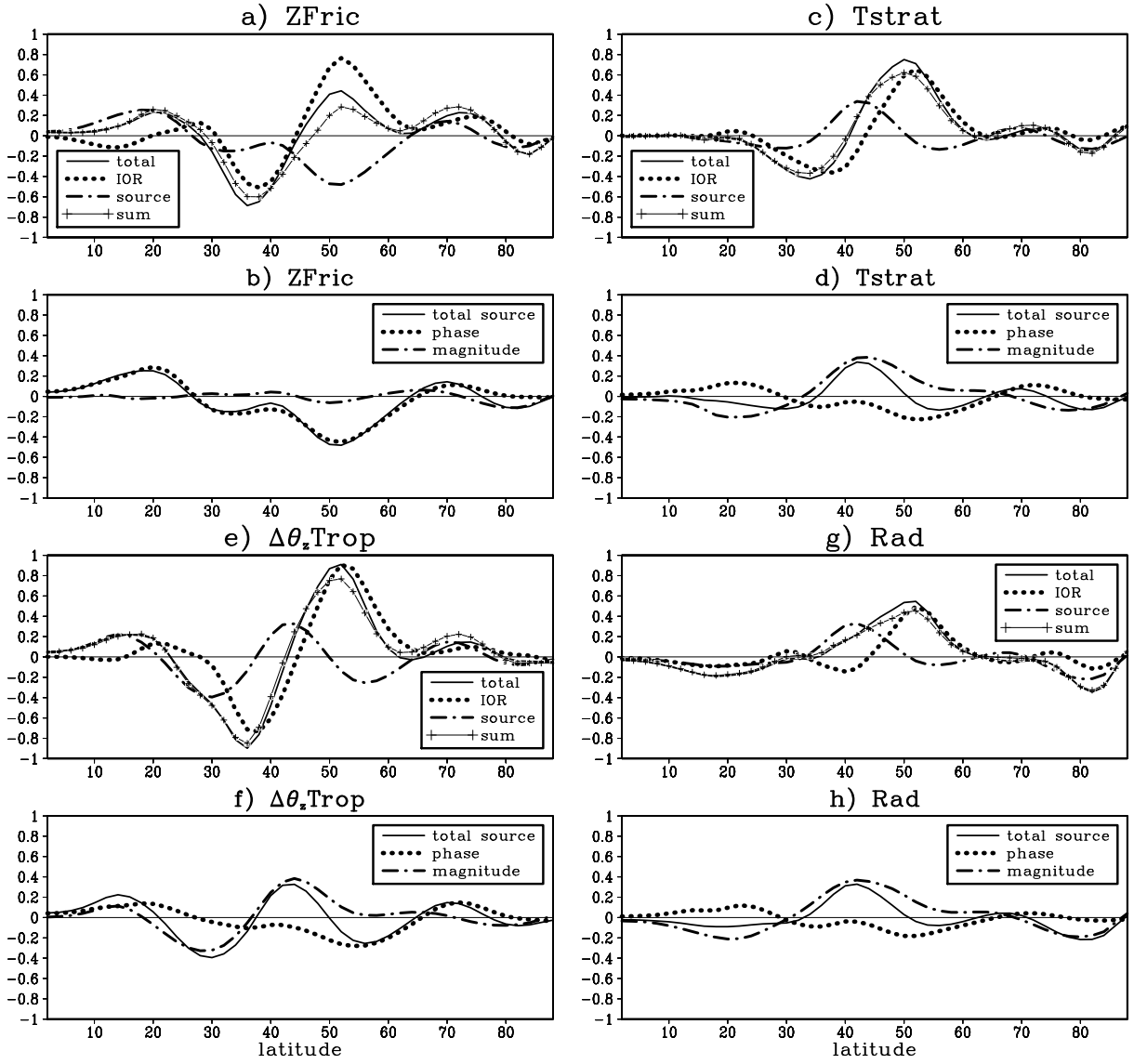

Figure 4: As in Fig. 3 but for the eddy momentum flux convergence ($= -\cos^{-2}\phi\partial_\phi(\overline{u'v'}\cos^2\phi)$) (m s^{-1} day^{-1}), and all lines are smoothed in latitude with a 1-2-1 filter.

coupled experiments are run with the IOR changes and the phase speed changes applied separately, the results confirm the results of the above analysis: 1) the jet shifts even further poleward when only the IOR changes and 2) $\bar{u}$ decreases (increases) on the poleward flank (in the subtropics) when the background flow only affects the phase speeds of the wave sources.

The contributions of the different mechanisms to the $\overline{u'v'}$ changes in phase speed space is shown in Fig. 5. For the spectra in the control run see Fig. 1. IOR changes lead to increases in $\overline{u'v'}$ that are concentrated on the poleward half of the jet, although there some positive anomalies in the subtopics in ZFRIC and RAD that are from changes in the critical level for zonal wavenumber 5. Phase speed changes shift the spectrum to the right leading to increases in $\overline{u'v'}$ at high phase speeds and decreases at low phase speeds. One expects some asymmetry in the breadth of the negative and positive anomalies (see discussion in section 5), but the degree of asymmetry requires another explanation (see Section 5). Source magnitude changes are relatively unimportant in ZFRIC where we do not directly force changes in the pole to equator temperature gradient. In TSTRAT and RAD (and in the other runs), the magnitude changes

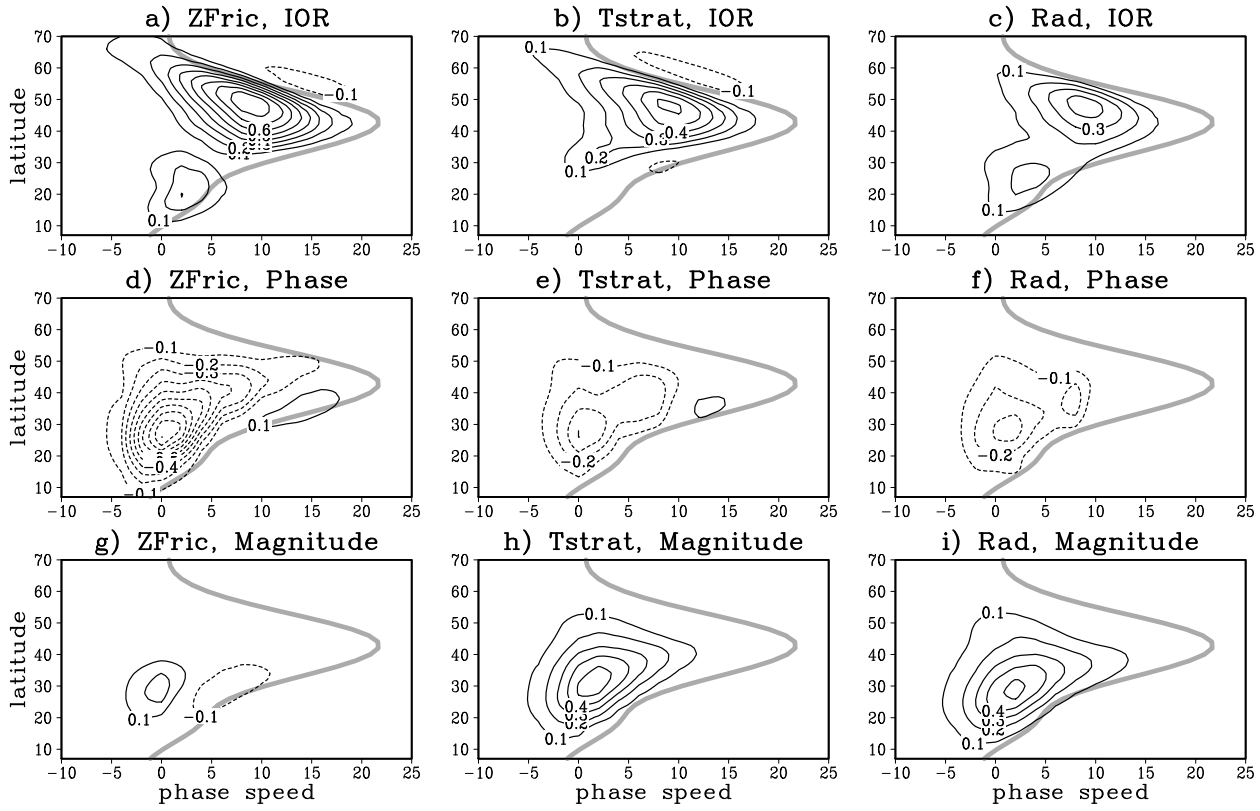

Figure 5: a) The change in the latitude/phase speed spectrum of eddy momentum flux due to changes in IOR in RWC for ZFRIC (m s^{-1}). The gray line is the critical level. The x-axis is angular phase speed in m s^{-1} at 45° (see section 2). b) As in (a) but for TSTRAT. c) As in (a) but for RAD. d) As in (a) but for the portion due to changes in the phase speed of the wave source. e) As in (d) but for TSTRAT. f) As in (d) but for RAD. g) As in (a) but for the portion due to changes in the magnitude of the wave source. h) As in (g) but for TSTRAT. i) As in (g) but for RAD.

look similar to the total momentum flux implying that the wave source increases are relatively insensitive to zonal wavenumber, latitude and phase. Closer inspection shows that there are slightly more increases at low phase speeds than at high phase speeds compared to the time-mean momentum flux (see Fig 5 in Lorenz (2014a)). In the next two sections, we provide a more detailed explanation of the dynamics behind the IOR and phase speed induced changes in $\overline{u'v'}$.

4. Wave Reflection

a. Introduction

In this section, we explore the specific mechanisms associated with IOR changes. These ideas will also explain more completely the behavior of the momentum fluxes in response to changes in phase speed.

Kidston and Vallis (2012) propose that changes in wave reflection (i.e. turning latitudes) are essential for shifting the jet poleward in a forced barotropic model. The evidence presented below suggests that changes in wave reflection are also essential in the RWC model and presumably the full GCM as well. To quantify regions of wave reflection in phase speed/latitude/wavenumber space we write (3) in Mercator coordinates (e.g. Hoskins and Karoly (1981)):

$$\frac{d^2\psi}{dy^2} + l^2\psi = 0, \tag{5}$$

where ψ is the complex streamfunction, l^2 is the index of refraction (4) and

$$\frac{d}{dy} = \cos\phi \frac{d}{d\phi}. \tag{6}$$

Note that unlike Hoskins and Karoly (1981) y is normalized by a in (5) and (6). An equation of the form (5) applies for each wavenumber and phase speed. When l^2 is positive (negative) solutions to (5) are oscillatory (evanescent) in y. As a wave propagates from

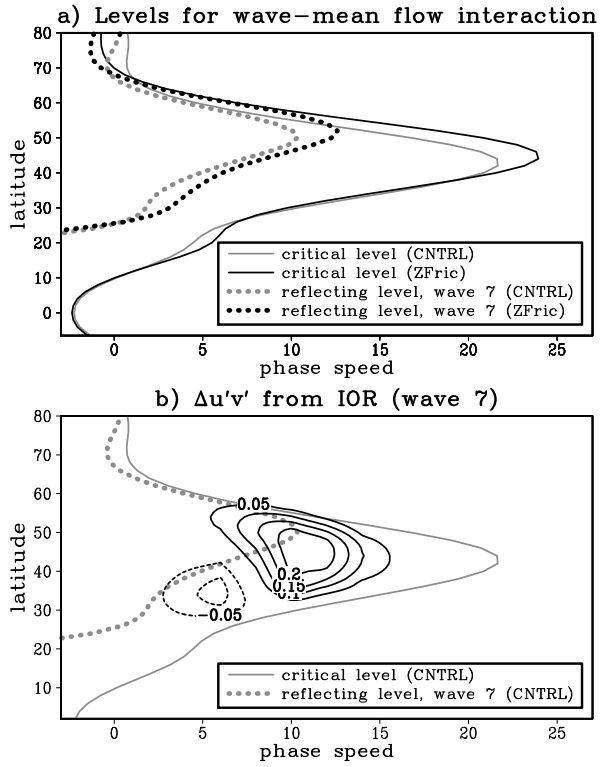

Figure 6: a) The critical level (solid) and the reflecting level for wavenumber 7 (dotted) for the control run (gray) and ZFRIC (black). The x-axis is angular phase speed in m s^{-1} at 45° (see section 2). b) The change in the latitude/phase speed spectrum of eddy momentum flux from IOR in RWC for ZFRIC (wavenumber 7) (m s^{-1}). The critical and reflecting level for the control run are shown.

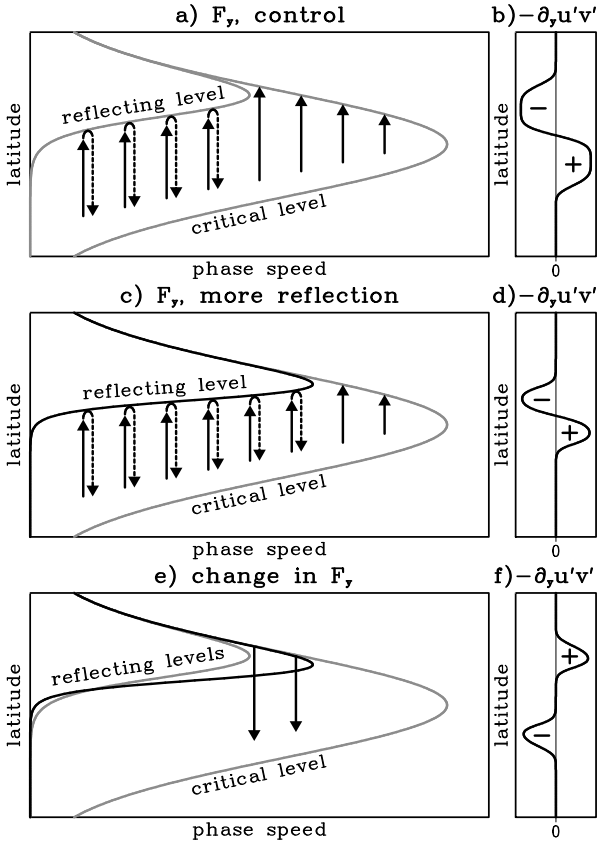

Figure 7: Schematic of the effect of the reflecting level on wave activity fluxes, F_y, in latitude/phase speed space (a,c,e) and the momentum flux convergence (integrated over phase speed) associated with these wave activity fluxes (b,d,f). The arrows point in the direction of the wave activity flux, which is *opposite* the momentum flux. The schematic *only* shows waves that initially propagate poleward. Reflected waves are dashed. The critical and reflecting levels are labeled. Note this schematic represents a single zonal wavenumber since the reflecting level is wavenumber dependent. a) Control F_y. b) Control momentum flux convergence integrated over phase speed. c) F_y for a state with more reflection. Note that the peak in the reflecting level extends to higher phase speeds. d) Momentum flux convergence for a state with more reflection. e) Solid arrows: net change in F_y. f) Net change in momentum flux convergence.

a region where $l^2 > 0$ toward a critical level (where $\bar{u}/(a\cos\phi) = c_\omega$), $l^2 \to \infty$ and in a linear dissipative model like our RWC model the wave is absorbed. Alternatively, when a propagating wave encounters an l^2 that approaches zero and then becomes negative, the wave is reflected (Hoskins and Karoly (1981)). In the latitude/phase speed plane the "reflecting level" is the set of points where $l^2 = 0$. Therefore, as a function of $\bar{u}$, β^* and m^2, the phase speed of the reflecting level is:

$$c_\omega = \frac{\bar{u}}{a\cos\phi} - \frac{\beta^* a\cos\phi}{m^2}. \qquad (7)$$

The critical and reflecting levels for wavenumber 7 for the control and ZFRIC run are shown in Fig. 6a. On the poleward flank of the jet, β^* is particularly small due to a combination of two effects 1) the planetary vorticity gradient approaches zero toward the pole and 2) the positive curvature in $\bar{u}$ ($= \bar{u}_{yy}$) is relatively large on the jet flanks (Kidston and Vallis (2010)). Hence, the reflecting level approaches the critical level on the poleward flank of the jet but is at significantly smaller phase speeds than the critical level at other latitudes. The key change in the reflecting level from the control run to the ZFRIC run is the increase in the range of phase speeds that encounter the reflecting level (Fig. 6a). A schematic of the mechanism, which involves the fate of initially poleward propagating waves, is shown in Fig. 7. The arrows in Figs. 7ace represent the horizontal wave activity fluxes, $F_y = -\overline{u'v'}\cos\phi$, which point in the direction opposite the momentum fluxes. The corresponding net momentum flux convergence associated with the F_y are shown

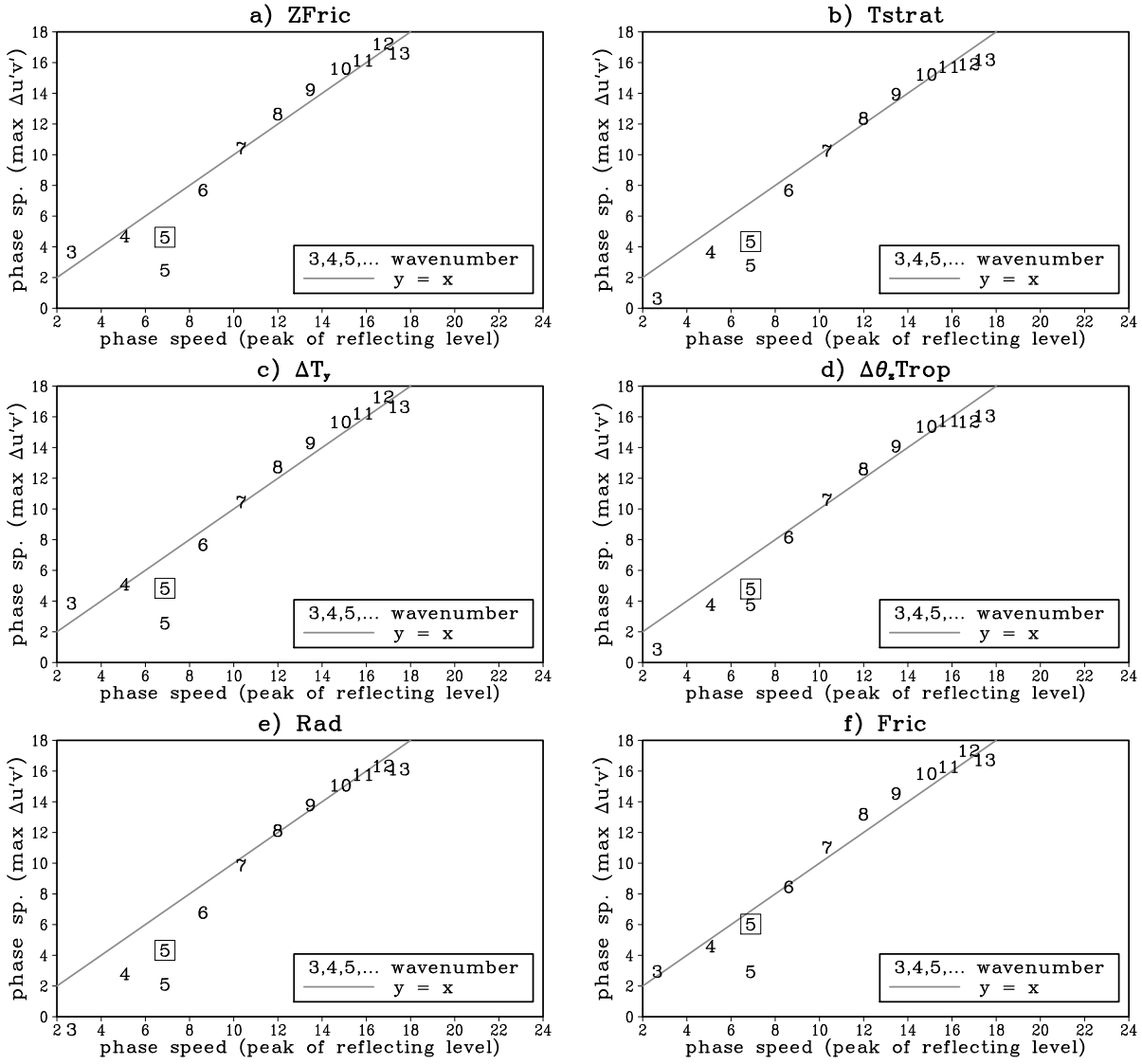

Figure 8: a) Scatter plot of angular phase speed of the peak of the reflecting level in the control run (x-axis) and the angular phase speed of the peak in the latitudinally-averaged eddy momentum change due to IOR (y-axis) for each zonal wavenumber from 3 to 13 (numbers). For the boxed number 5, the momentum flux change is latitudinally-averaged poleward of 40° rather than globally. The units of the angular phase speed are m s^{-1} at 45° (see section 2). b) As in (a) but for TSTRAT. c) As in (a) but for ΔT_y. d) As in (a) but for $\Delta\theta_z$TROP. e) As in (a) but for RAD. f) As in (a) but for FRIC.

in Figs. 7bdf. As the maximum c of the reflecting level increases, more waves reflect instead of being absorbed at the critical level on the poleward flank of the jet (Fig. 7c). The net effect is an increase in the poleward momentum fluxes across the jet (Fig. 7e) that help maintain the jet in its poleward shifted location (Fig. 7f). The actual change in $\overline{u'v'}$ from IOR changes is shown in Fig. 6b. The increase in poleward momentum fluxes is located near the maximum c of the reflecting level, which is consistent with the reflecting level blocking access to the critical level on the poleward flank of the jet (we will discuss the decreases in $\overline{u'v'}$ below). The change in $\overline{u'v'}$ tracks the reflecting level for other wave numbers as well (Fig. 8). Here we plot the phase speed of the peak of the reflecting level in the control run versus the phase speed of the maximum $\overline{u'v'}$ change, where $\overline{u'v'}$ is first (cosine-weighted) averaged over latitude. Except for wavenumber 5, the location of the mean reflecting level appears to determine where $\overline{u'v'}$ changes. For wavenumber 5, it appears that critical level dynamics near the *equatorward* flank of the jet are leading to $\overline{u'v'}$ changes there (not shown). Therefore if we average $\overline{u'v'}$ from 40° pole-

ward then wavenumber 5 agrees significantly better with the other wavenumbers (see boxed number 5 in Fig. 8).

b. Explicit reflectivity calculations

Given that the width of the barrier associated with the reflecting level (i.e. the region where the waves are evanescent and $l^2 < 0$) is not very large, it may seem that waves would have little trouble tunneling through the barrier and reaching the critical level anyway. For example, in Fig. 6b the momentum flux anomalies extend to the far side of the reflecting level demonstrating that the reflecting level contrains the momentum fluxes less than the critical level. Here we explicitly calculate a reflectivity coefficient associated with this barrier and show that the changes in reflectivity are quite similar to the changes in momentum flux. Consider the latitudinal profile of l^2 for one wavenumber and phase speed (Fig. 9a). Toward the critical levels on the flanks of the jet, l^2 approaches positive infinity and then abruptly changes sign to negative infinity on the evanescent side of the critical level. The features of interest here are the non-singular zero crossings and region of evanescence between the critical levels, which can potentially reflect waves. To isolate the effect of the reflective region we "truncate" the l^2 profile so that regions where $l^2 > l_0^2$ and regions beyond the critical levels are given the value l_0^2, where l_0^2 is constant threshold (Fig. 9b). Here l_0^2 is the value of l^2 halfway between the critical level on the equatorward side and either the reflecting level or critical level on the poleward side, which ever comes first. The general results that follow are insensitive of the details that determine l_0^2. To calculate the reflectivity/transmissivity of the barrier we integrate the truncated version of (5) as an initial value problem instead of a boundary value problem. We start the integration poleward of the reflective region with an arbitrary non-zero complex initial condition and a slope that is consistent with a poleward propagating wave ($l > 0$). We then integrate (5) backward toward the equator to find the relative amplitudes of the poleward and equatorward propagating waves on the opposite side of the barrier. The ratio of the equatorward to poleward wave activity flux on the equator side of the barrier is the reflectivity coefficient associated with the barrier and the ratio of the poleward wave activity flux poleward of the barrier to the poleward wave activity flux equatorward of the barrier is the transmissivity coefficient. Note this is precisely the same technique used to calculate the reflectivity/transmissivity of a quantum mechanical barrier where l^2 is analogous to the *negative* of the potential energy minus the energy and the wave activity flux is analogous to the probability current. The details and rationale of the calculation are given in Appendix B.

The reflectivities of the profiles shown in Fig. 9b are 0.24 and 0.70 for the control and the ZFRIC runs, respectively. The reflectivity for a range of phase speeds for wavenumber 7 is shown in Fig. 9c. The locations of the maximum c of the reflecting levels for the control and ZFRIC are shown by the vertical line. As expected, the transition from perfect reflection to perfect transmission is not abrupt but instead occurs over a range of approximately 7 m s^{-1}. Moreover, because of tunneling, the largest change in reflectivity occurs at phase speeds slightly less than the phase speed of the "reflecting level" maximum (short dashed vertical line). Similarly, the change in reflectivity is shifted toward lower phase speeds relative to the new transmission region as estimated by the reflecting level maxima (i.e. between the two vertical lines, Fig. 9d). The magnitude of the reflectivity change is over 0.4 at $c = 10$ m s^{-1} and the structure corresponds well to the change in momentum flux due to IOR, where the momentum flux is first (cosine-weighted) averaged over the latitudes 40° to 60° (the details of the averaging are not important). Taken together with Fig. 8, these results suggest that the increases in poleward momentum fluxes across the jet that are essential for maintaining the poleward shift are primarily caused by increased wave reflection at the poleward flank of the jet. This is the same mechanism proposed by Kidston and Vallis (2012) and is very closely related to the results of Barnes and Hartmann (2011). We also should point out that the reason the $\overline{u'v'}$ response to $\bar{u}$ seems relatively simple is that we have isolated the effect of IOR changes. In the GCM, a similar $\bar{u}$ perturbation also changes the phase speed of the waves, making the response much harder to interpret.

We now describe a simple diagnostic based on reflectivity calculation above to help better quantify the role of reflection.[4] For the diagnostic, the phase speed profile

[4]To apply the reflectivity diagnostic to a wider range of phase speeds and wavenumbers, we modify the calculation of l_0^2, which before was an average over a region bounded on the poleward side by either the critical level or the reflecting level, which ever comes first (i.e. is further equatorward). To make the reflectivity more robust, the l^2 averaging region can be bounded on the poleward side by a relative minima in the angular velocity, $\bar{u}/\cos(\phi)$, provided this comes first.

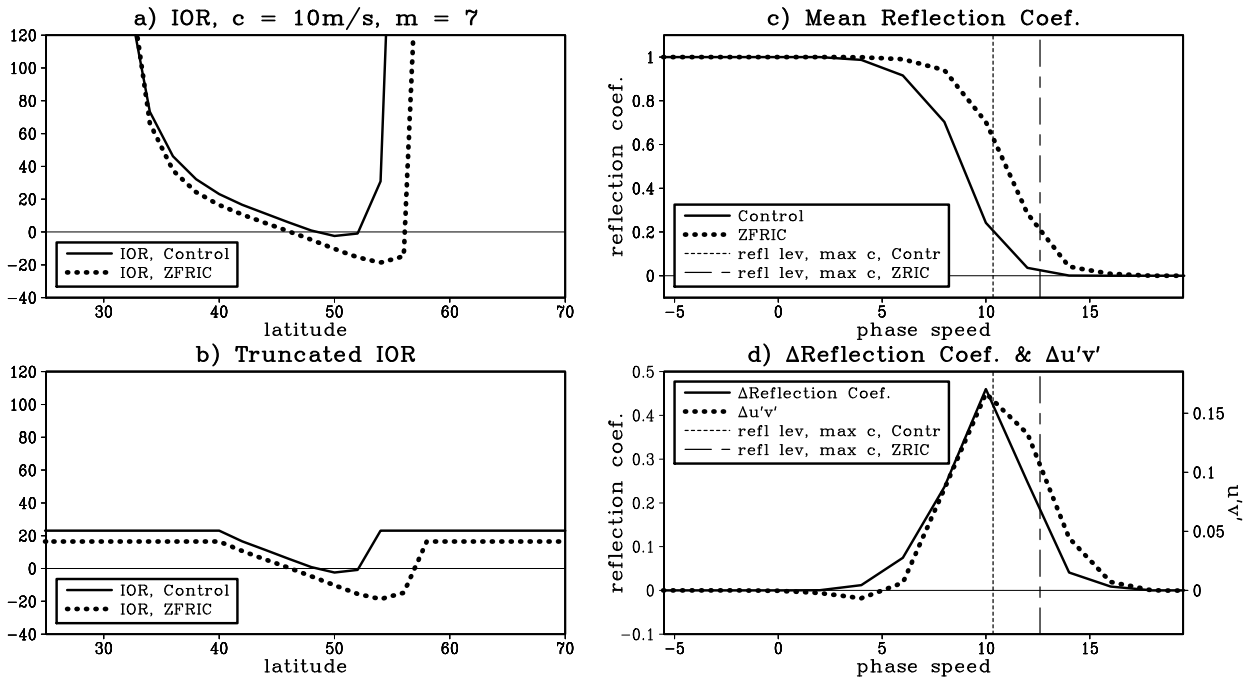

Figure 9: a) The latitude profile of the non-dimensional index of refraction for c = 10 m s^{-1} and m = 7 in the control (thin solid) and the ZFRIC (thick dotted) run. b) As in (a) but for the "truncated" index of refraction (see text). c) The reflectivity coefficient associated the poleward half of the jet as a function of angular phase speed for m = 7. The control reflectivity is thin and solid and the ZFRIC reflectivity is thick and dotted. The vertical lines denote the angular phase speed of the peak in the reflecting level for the control (short dashed) and ZFRIC (long dashed) runs. The units of the angular phase speed are m s^{-1} at 45° (see section 2). d) The angular phase speed profile of the change in reflectivity (thin solid) and the change in RWC eddy momentum flux due to IOR averaged from 40 to 60° (thick dotted). The vertical lines are the same as in (c). The units for the momentum flux spectrum are m s^{-1}.

of the reflectivity change, $r(c,m)$, determines the phase speed profile of what we call the $\overline{u'v'}$ profile due to reflection. The scaling of the reflectivity profile, $\gamma(m)$, is determined from simple linear regression over the variations in c:

$$\xi = \gamma r + b, \tag{8}$$

where ξ is either the positive or negative portion of the momentum flux integrated over latitude depending on the sign of the reflectivity change, r:

$$\xi(c,m) = \begin{cases} \int_{0^\circ}^{90^\circ} \max(\overline{u'v'},0)\cos(\phi)d\phi & \text{if } r(c,m) > 0 \\ \int_{0^\circ}^{90^\circ} \min(\overline{u'v'},0)\cos(\phi)d\phi & \text{if } r(c,m) < 0 \\ 0 & \text{if } r(c,m) = 0. \end{cases} \tag{9}$$

The linear regression is performed separately for each wavenumber, m. For the important wavenumbers (m = 3 through 8), the change in momentum flux closely resembles the reflectivity and the linear fit (8) explains 90% of the variance in ξ. The above diagnostic, γr, only defines the effect of reflection in the c-m plane. In most cases, the full latitudinal profile of the "$\overline{u'v'}$ due to reflection" is estimated by scaling the latitudinal profile $\overline{u'v'}$ by $\alpha = \gamma r/\xi$, where we only scale the portion of $\overline{u'v'}$ that is the same sign as r. We also restrict the scaling to be nonzero only when r explains at least half the variance in ξ (i.e. the correlation associated with (8) exceeds 0.707). The scaling is perform for each c and m. Due to the indiscriminate use of the full latitudinal profile of $\overline{u'v'}$ (provided the $\overline{u'v'}$ profile in c matches the reflectivity change, of course), it is possible that the reflectivity diagnostic is including effects from the critical level on the equatorward flank as well. Using a model of the critical level described in Lorenz (2014b), however, we find that this effect is small in the experiments we have considered.

Using this reflectivity diagnostic we remove the effect of reflection from the $\overline{u'v'}$ changes due to IOR. When we "remove" the reflection, the $\overline{u'v'}$ change (from IOR) is reduced dramatically in most of the perturbed experiments (Fig. 10). According to this analysis, the change in reflectivity has the least effect for the TSTRAT run, although even here it accounts for over half the response.

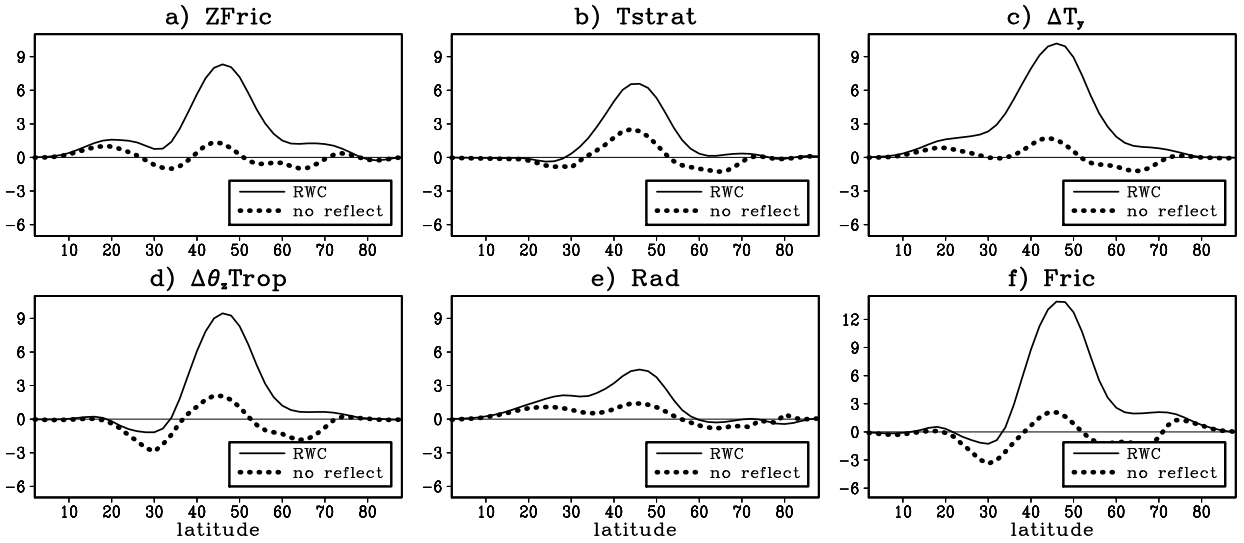

Figure 10: a) The change in eddy momentum flux from changes in IOR in RWC (thin solid) and the residual of the change in eddy momentum flux from IOR after the part linearly related to the reflectivity is removed (thick dotted). The units are $m^2\ s^{-2}$. b) As in (a) but for TSTRAT. c) As in (a) but for ΔT_y. d) As in (a) but for $\Delta\theta_z$TROP. e) As in (a) but for RAD. f) As in (a) but for FRIC.

c. Role of zonal wind versus vorticity gradient

In the discussion above we have argued that the maximum c of the reflecting level increases and this causes more waves to be reflected, but we have not explicitly discussed the changes in the background $\bar{u}$ and β^* and how they effect the reflecting level through (7). The changes in $\bar{u}$ are dominated by an increase at 52° ,which is on the poleward flank of the mean jet (= 42°) (Fig. 11). In general, the changes in β^* tend to be positively correlated with the changes in $\bar{u}$ although, as expected, the β^* changes tend to be of smaller scale (Fig. 11). At the latitude of the maximum in the reflecting level (= 50° for wavenumber 7), the changes in $\bar{u}$ and β^* are the same sign. Therefore, according to (7), the increases in $\bar{u}$ (β^*) poleward of the mean jet act to increase (decrease) in the range of phase speeds reflected on the poleward flank. This is demonstrated in Fig. 11b, which shows the changes in reflecting level for wavenumber 7 when the $\bar{u}$ or β^* changes are applied separately.

The opposite effect of $\bar{u}$ and β^* on the reflecting level (in this case) implies that the $\bar{u}$ and β^* changes would have opposite effects on the $\overline{u'v'}$ changes if the $\bar{u}$ and β^* changes were applied separately. We find that this is indeed the case (Fig. 12). In all cases, including the two runs not shown here, the $\bar{u}$ changes lead to strong positive momentum fluxes across the jet (mean jet latitude = 42°) that are consistent with a poleward shifted jet. Moreover, in all cases the β^* changes lead to the opposite $\overline{u'v'}$ re-

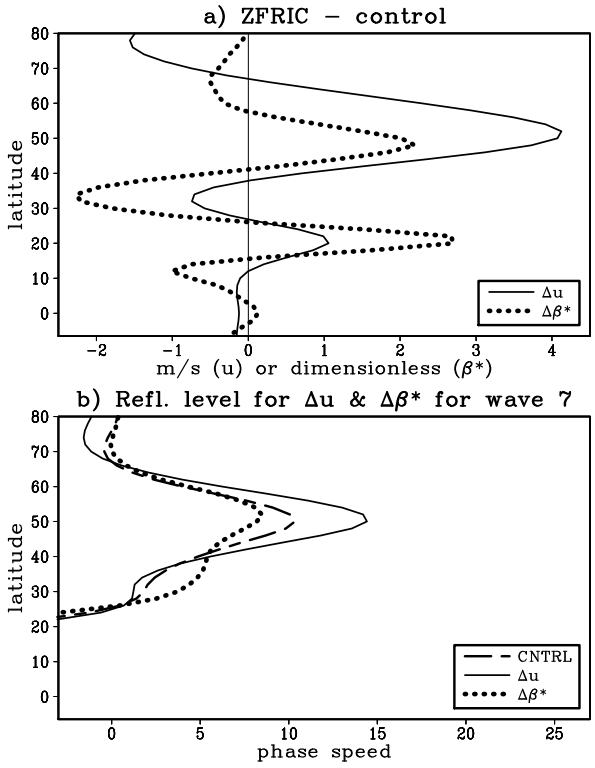

Figure 11: a) The change in $\bar{u}$ and β^* in the ZFRIC run relative to the control. The β^* plotted here is scaled by $Da\cos(\phi)$, where D is the length of day. b) The reflecting level for wavenumber 7 in the control run (dashed), and the reflecting level in ZFRIC when $\bar{u}$ (thin solid) or β^* (thick dotted) are applied separately in (5).

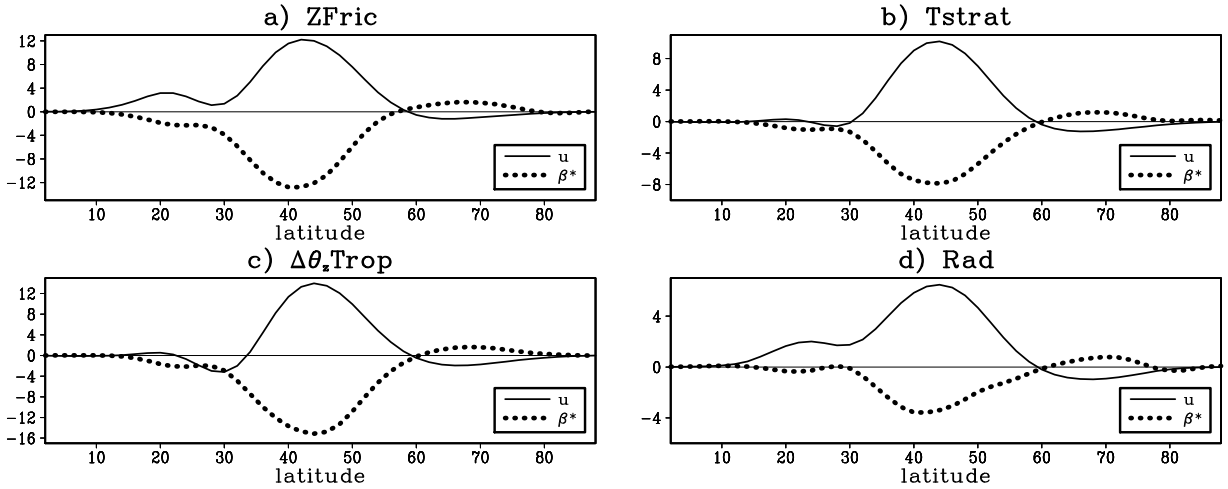

Figure 12: The change in eddy momentum flux from changes in IOR in RWC when the $\bar{u}$ (thin solid) or β^* (thick dotted) changes are applied separately. a) ZFRIC. b) TSTRAT. c) $\Delta\theta_z$TROP. d) RAD.

sponse, which tends to oppose the poleward shift in the jet. We should note that linear super-position does not hold in this case: the response to both $\bar{u}$ and β^* together does not equal the sum of the responses to $\bar{u}$ and β^* separately. However, the response to $\bar{u}$ and β^* separately is so robust that we believe it is still useful to consider the response to each individually.

In summary, we argue that the key latitude for changing the reflectivity of the poleward flank is the latitude of the maximum of the reflecting level. Unlike the critical level, the reflecting level depends on the zonal wavenumber so the maximum of the reflecting level varies with wavenumber as well. The $\overline{u'v'}$ response is dominated by wavenumbers 4-8 which have peak reflecting levels varying from 56° (for m = 4) to 48° (for m = 8). Hence the "average" peak is at 52° and this is the latitude where reflection is most sensitive to $\bar{u}$ and β^* perturbations (Lorenz (2014b)). Not coincidentally, 52° is also the location of the poleward center of action of EOF1 (see Lorenz (2014b)). In Lorenz (2014b), we will also discuss how a stronger jet evolves toward the poleward shifted jet that is optimally located to excite the reflecting level.

d. Decreases in momentum flux from IOR

We now provide a possible explanation for the relatively weak decreases in $\overline{u'v'}$ in Fig. 6b. We argue above that most of the effects of $\bar{u}$ on $\overline{u'v'}$ are caused by the reflecting level (and the critical level, see Lorenz (2014b)). The reduction in $\overline{u'v'}$ in Fig. 6, however, appears related to changes in group velocity in the interior of the

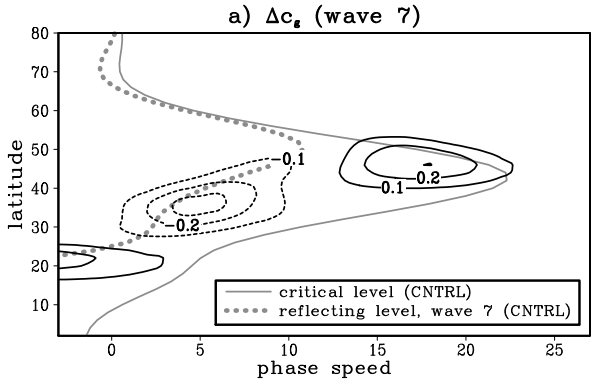

Figure 13: The change in meridional group velocity for wavenumber 7 in ZFRIC. The group velocity has been smoothed with two applications of a local 9-point smoother. The units are degrees per day. The critical and reflecting levels for the control run are shown.

propagating region. The (smoothed) group velocity of the waves is reduced in the same region as the reduction in $\overline{u'v'}$ (compare Fig. 13 with Fig. 6). A reduced group velocity reduces $\overline{u'v'}$ because it gives more time for the dissipation to act. The reduction in group velocity is related to the expansion of the reflecting level to higher phase speeds in this region (Fig. 6a), which is synonymous with a contraction of the wave propagation region. The increases in the group velocity in Fig. 13 have little impact because the mean $\overline{u'v'}$ is weak in these regions (not shown).

5. Response to changes in phase speed

Current ideas on the effect of phase speed changes on momentum fluxes emphasize the equatorward propagating waves and the critical level on the equatorward flank of the jet (Chen et al. (2007)). To help describe these ideas, consider the schematic of the mean horizontal wave activity fluxes, $F_y = -\overline{u'v'}\cos\phi$, in Figs. 14ace. The corresponding net momentum flux convergence associated with the F_y are shown in Figs. 14bdf. The wave activity fluxes in the mean state (Fig. 14a) originate near the jet maximum, predominantly propagate equatorward and then irreversibly break and decay near the critical level (gray line). If phase speeds of the waves increase, the spectrum shifts to the right towards faster phase speed leading to increases at high phase speeds and decreases at low phase speeds (Fig. 14c). In shifting to the right, the waves are still constrained to stop at their critical latitude, which they reach slightly sooner compared to the control case. Therefore, there is a net decrease in equatorward wave activity at all latitudes where there is a critical latitude for the waves. This leads to an eddy forcing dipole that is restricted to the equatorward flank of the jet (Fig. 14d). Unfortunately, this scenario does not appear to fully explain the effect of changes in phase speed seen in Figs. 3, 4 and 5. For example, summing over phase speed, the effect of phase speed on $\overline{u'v'}$ in the RWC model is not restricted to the equatorward flank of the jet (see dotted lines in Figs. 3bdfh and 4bdfh). Instead, the reductions in $\overline{u'v'}$ extend to the poleward flank and actually act to directly oppose the poleward shift. Similarly, looking at the phase speed/latitude spectrum (Fig. 5), the decreases in $\overline{u'v'}$ at low phase speeds dominate over the increases in $\overline{u'v'}$ to an extent not suggested by the schematic (Fig. 14c).

The explanation for these discrepancies involves the phase speed-selective reflecting level on the poleward flank of the jet (see section 4). Increased phase speeds mean more waves are absorbed instead of reflected on the poleward flank of the jet. The net result is a reduction in momentum fluxes across the jet in addition to the reduction on the equatorward flank suggested by Chen et al. (2007) (Fig. 14e). Because the location of the reflecting level is wavenumber dependent, it is easiest to see the effect of the reflecting level when considering a single wavenumber. Fig. 15 shows the change in wave source due to changes in phase speed (see section 3) and momentum fluxes forced by these wave source changes

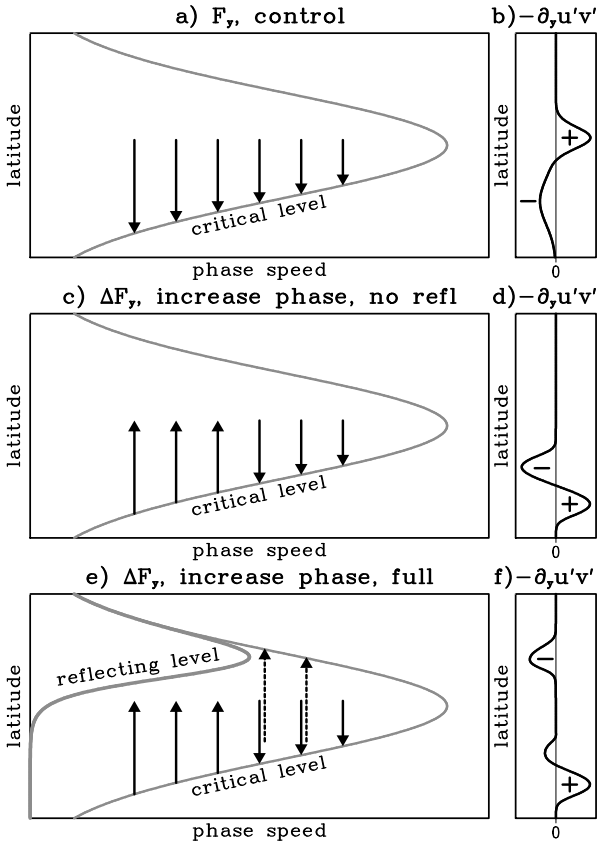

Figure 14: Schematic of the effect of changes in wave activity source phase speeds on wave activity fluxes, F_y, in latitude/phase speed space (a,c,e) and the momentum flux convergence (integrated over phase speed) associated with these wave activity fluxes (b,d,f). The arrows point in the direction of the wave activity flux, which is *opposite* the momentum flux. The critical and/or reflecting levels are labeled. a) F_y in a control run where only initially equatorward propagating waves are considered. b) Momentum flux convergence integrated over phase speed where only initially equatorward propagating waves are considered. c) The change in F_y in response to increases in phase speed where only initially equatorward propagating waves are considered. d) The change in momentum flux convergence in response to increases in phase speed where only initially equatorward propagating waves are considered. e) The full change in F_y in response to increases in phase speed. Higher phase speeds mean that poleward propagating waves near the peak of the reflecting level that were once reflected are now absorbed at the critical level on the poleward flank of the jet. The net effect is the response in (c) *minus* the response in Fig. 7e. Note this plot represents a single zonal wavenumber since the reflecting level is wavenumber dependent. f) The net momentum flux convergence associated with (e).

for wavenumber 7. The change in wave source shows the characteristic dipole consistent with a simple shift toward higher phase speeds (Fig. 15a). While the change in $\overline{u'v'}$ (Fig. 15b) shows some similarities with the wave source on the equatorward half of the jet, $\overline{u'v'}$ decreases

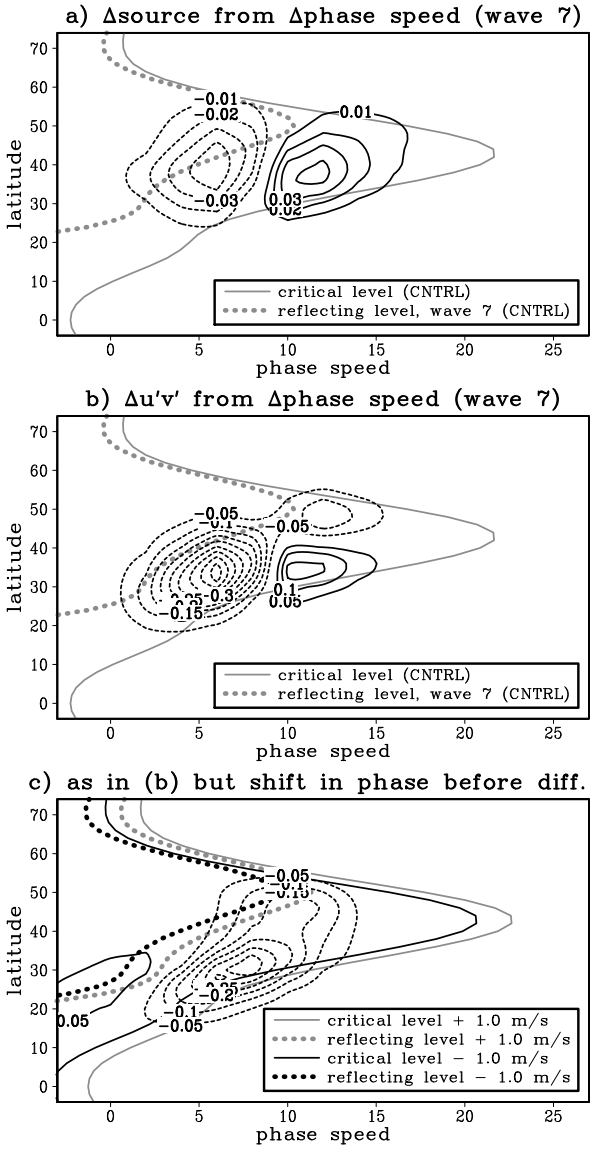

Figure 15: a) The change in the latitude/phase speed spectrum of the wave activity source due to changes in phase speed for wavenumber 7. The critical and reflecting levels for the control run are shown. The x-axis is angular phase speed in m s^{-1} at 45° (see section 2). b) The change in the latitude/phase speed spectrum of the RWC eddy momentum flux due to changes in phase speed. c) Same as in (b) but the control momentum flux is transformed 1.0 m s^{-1} to the right and the ZFRIC momentum flux is transformed 1.0 m s^{-1} to the left before the difference is calculated. The critical and reflecting levels under the same transforms are also shown.

on the poleward flank of the jet in the same region where we expect the reflecting level to impact $\overline{u'v'}$ (see Fig. 6).

The effects of the reflecting level and the critical level on the response to phase speed changes are easiest to see by first transforming the $\overline{u'v'}$ in phase speed before taking the difference. Therefore, we shift the control run spectrum 1.0 m s^{-1} to the right and the response (to increased phase speeds) spectrum 1.0 m s^{-1} to the right. Applying this transform to the wave source nearly cancels the phase speed increase and results in a very weak response (not shown). The application of this transform to $\overline{u'v'}$ is shown in Fig. 15c together with the critical and reflecting levels under the transformations. The situation is now analogous to the case of constant wave source but a background flow changing from the gray lines to the black lines. The (effective) change in the critical level on the equatorward flank of the jet means waves do not propagate as far into the subtropics and therefore $\overline{u'v'}$ decreases in the vicinity of the critical level. There is an additional decrease in the vicinity of the reflecting level on the poleward flank of the jet. This decrease is consistent with the decrease in the maximum phase of the reflecting level, which means more poleward propagating waves are absorbed instead of reflected on the poleward flank of the jet. There are also relatively weak increases in $\overline{u'v'}$ at low phase speeds in the vicinity of the reflecting level. Since the region of wave propagation lies between the critical level and the reflecting level, these increases are likely the result of an expansion of the wave propagation region in this location of phase speed/latitude space. In summary, it is the combination of the critical level on the equatorward flank and the reflecting level on the poleward flank that gives rise to the broad latitudinal profile of the phase speed induced momentum flux changes. Because of the reflecting level in particular, these fluxes actually act to decrease the $\bar{u}$ anomalies associated with the poleward shift (Fig. 14f).

The fact that the changes in IOR and the increases in phase speeds impact wave reflection in opposite ways begs the question: why is the IOR effect larger? Based on experiments in Lorenz (2014b), we believe that IOR dominates because the phase-speed-induced $\overline{u'v'}$ is an integrator of $\bar{u}$ across the entire width of the wave source region while IOR is not. For example, a *local* $\bar{u}$ anomaly on the poleward flank changes the reflectivity for *all* waves propagating toward the poleward flank of the jet. This same anomaly results in a significantly smaller change in the net phase speed of the waves propagating toward the poleward flank because some of these waves have source latitudes relatively far removed from the local $\bar{u}$ anomaly.

6. Discussion and Conclusions

We use RWC to diagnose and understand poleward shifted jets in an idealized GCM using the GCM's convergence of the vertical EP flux (Edmon et al. (1980)) in the upper troposphere as the wave activity source. First we separate the contributions of the source magnitude, the source phase speed and the Index of Refraction (IOR) (i.e. background flow with no changes in source) to the momentum flux changes. We find that (1) changes in IOR are responsible for maintaining the poleward shifted jet, (2) source phase speed changes directly oppose the poleward shifted jet and (3) source magnitude changes are either negligible or else act to strengthen the mean jet.

As proposed by Kidston and Vallis (2012), we find that the key role of IOR is a result of changes in the reflectivity of the poleward flank of the jet. IOR affects the waves via a selective "reflecting level" on the poleward flank of jet: for a given wavenumber, low phase speed waves are reflected but high phase speed waves are absorbed at the critical level on the poleward flank of jet. When $\bar{u}$ increases on the poleward flank of the jet, the peak of the reflecting level shifts to higher phase speeds and thus a wider range of poleward propagating waves encounter a reflecting level instead of a critical level on the poleward flank. The increased wave reflection leads to increased equatorward propagating waves (and therefore poleward momentum flux) across the jet (Kidston and Vallis (2012)).

Chen et al. (2007) emphasize the effect of phase speed changes on the equatorward propagating waves and the critical level on the equatorward flank: an increase in wave phase speed causes the equator-side critical line to move poleward and therefore reduces momentum fluxes on the equatorward flank of the jet. This leads to negative $\bar{u}$ forcing directly equatorward of the jet and positive forcing deeper in the subtropics. In the presence of a selective reflecting level, however, higher phase speeds also imply more wave absorption and less wave reflection on the poleward flank of the jet. The net result is a reduction in momentum fluxes across the jet in addition to the reduction on the equatorward flank. This also means that the negative $\bar{u}$ forcing from phase speed changes is actually on the poleward flank of the jet and therefore directly opposes the poleward shift.

In the experiments where the meridional temperature gradient is increased in some way, the increases in the magnitude of the wave activity sources act to strengthen the mean jet. While this may seem peripheral to the poleward shift, we believe that in some cases the source magnitude increases are essential for acting to strengthen the jet so that the reflecting level dynamics can play a role. For example, the direct "radiative" response to increased pole-to-equator temperature gradient in the Held and Suarez (1994) GCM is predominantly increased $\bar{u}$ in the subtropics.[5] We believe that the source magnitude increases ensure that these perturbations predominantly increase $\bar{u}$ in the mid-latitudes rather than in the subtropics. This is a topic of future research. Note that source magnitude increases should not be viewed as essential for the poleward shift in general because the jet moves poleward when the zonal-mean component of friction is reduced.

The focus of this paper is on mechanisms that maintain the jet in its poleward shifted position. In a companion paper (Lorenz (2014b)), we will explore the mechanisms that cause stronger jets to shift poleward. Like Kidston and Vallis (2012), we find that reflection plays a key role in the response to stronger jets as well. In this paper, we have not discussed critical level dynamics on equatorward flank of jet except in relation to phase speed changes. This is because the $\bar{u}$ changes analyzed here are predominantly on poleward flank of the jet. In Lorenz (2014b), we explore the response to arbitrary $\bar{u}$ anomalies and we find that critical level dynamics is important on the subtropical flank of the jet. This may be relevant for the response to El Niño versus global warming (Lu et al. (2008)).

Because the peak of the reflecting level is on the poleward flank of the mid-latitude jet, the jet latitude is especially sensitive to $\bar{u}$ anomalies on the poleward flank of the jet. This is likely very relevant for troposphere-stratosphere interaction for mean states with a stratospheric polar night jet just poleward of tropospheric mid-latitude jet as in observations. The results here suggest that positive (negative) anomalies in the lower stratosphere increase (decrease) the range of tropospheric waves that are reflected, resulting in increased (decreased) momentum fluxes across the jet and the positive (negative) phase of the annular mode. Usually this type of wave-mean flow interaction is diagnosed with IOR in the latitude-pressure plane, which implicitly assumes that the wave packets transporting momentum are localized in upper troposphere. As mentioned in the Introduc-

[5] By direct "radiative" response we mean that we fix eddy fluxes at control values while we increase the pole-to-equator temperature gradient in a zonally symmetric version of the GCM.

tion, however, using upper troposphere potential vorticity (PV) gradients results in a poor simulation of the mean climate. This suggests that the barotropic version of the IOR is more appropriate for diagnosing stratosphere/troposphere interaction.

Acknowledgments.

The author would like to thank Joe Kidston, Paulo Ceppi, Jian Lu, Dan Vimont and an anonymous reviewer for their helpful comments and suggestions on the manuscript. This research was supported by NSF grants ATM-0653795 and AGS-1265182.

APPENDIX

Calculating the reflectivity coefficient

In this Appendix, we describe the calculation of the reflectivity coefficient associated with the truncated l^2 profiles described in section 4b (e.g. Fig. 9b). The calculations are much easier to explain if one assumes a particular hemisphere at the outset (poleward propagating waves have opposite sign l depending on the hemisphere). Therefore we assume we are in the Northern Hemisphere from now on. Also, the term "barrier" is used for the region of low l^2.

Given a northward travelling wave south of the barrier, we want to know how much wave activity is reflected and how much is transmitted. Therefore, the desired solution has both northward and southward propagating waves south of the barrier but only northward propagating waves north of the barrier. To achieve this desired solution, we integrate (5) as an initial value problem from the north side of the barrier with an initial value and initial derivative consistent with only northward propagating waves. The initial amplitude of the (complex) ψ is arbitrary and for simplicity is assigned the value of one at a point y_0 that is north of the barrier. The general solution of ψ north of the barrier (where l is constant) includes a term proportional to $\exp(ily)$ and a term proportional to $\exp(-ily)$. The relevant northward propagating wave is the positive l solution and therefore $\psi = \exp(il(y - y_0))$ and the initial derivative at y_0 is il. We then integrate (5) southward with the fourth-order Runge-Kutta method. The y-grid is the non-uniform Mercator coordinate grid obtained by simply transforming the uniform 2° latitude grid used for the GCM and the RWC model. After integrating southward past the barrier, the relative amplitudes of the northward and southward wave activity fluxes can be calculated from ψ and $d\psi/dy$. The total wave activity flux, F, is proportional to:

$$F = -\Re\left(vu^*\right) = -\Re\left((im\psi)\left(-\frac{d\psi}{dy}\right)^*\right) = \Re\left(im\psi\frac{d\psi^*}{dy}\right), \tag{A1}$$

where u and v are the eddy zonal and meridional winds, respectively. In the constant l region south of the barrier, ψ can be written in the following form:

$$\psi(y) = A\exp(ily) + B\exp(-ily), \tag{A2}$$

where A and B are constants. Substituting (A2) into (A1) and simplifying:

$$F = lmAA^* - lmBB^*, \tag{A3}$$

where the first (second) term is the wave activity flux from the northward (southward) propagating waves. The reflectivity coefficient is simply the ratio of the (absolute value of the) southward to northward flux evaluated south of the barrier:

$$\text{reflectivity coefficient} = \frac{BB^*}{AA^*}. \tag{A4}$$

The constant A can be found from ψ and its first derivative by assuming the form (A2) and adding $il\psi$ and $d\psi/dy$:

$$A = \frac{1}{2}\left(\psi - \frac{i}{l}\frac{d\psi}{dy}\right)\exp(-ily). \tag{A5}$$

Likewise

$$B = \frac{1}{2}\left(\psi + \frac{i}{l}\frac{d\psi}{dy}\right)\exp(ily). \tag{A6}$$

Therefore

$$\text{reflectivity coefficient} = \frac{|\psi + \frac{i}{l}\frac{d\psi}{dy}|^2}{|\psi - \frac{i}{l}\frac{d\psi}{dy}|^2}, \tag{A7}$$

where ψ and $d\psi/dy$ are evaluated at a point south of the barrier.

REFERENCES

Barnes, E. A. and D. L. Hartmann, 2011: Rossby wave scales, propagation, and the variability of eddy-driven jets. *J. Atmos. Sci.*, **68**, 2893–2908.

Barnes, E. A., D. L. Hartmann, D. M. W. Frierson, and J. Kidston, 2010: Effect of latitude on the persistence of eddy-driven jets. *Geophys. Res. Lett.*, **37**, L11 804.

Butler, A. H., D. W. J. Thompson, and R. Heikes, 2010: The steady-state atmospheric circulation response to climate change-like thermal forcings in a simple general circulation model. *Journal of Climate*, **23**, 3474–3496.

Chen, G., I. M. Held, and W. A. Robinson, 2007: Sensitivity of the latitude of the surface westerlies to surface friction. *J. Atmos. Sci.*, **64**, 2899–2915.

Chen, G. and P. Zurita-Gotor, 2008: The tropospheric jet response to prescribed zonal forcing in an idealized atmospheric model. *J. Atmos. Sci.*, **65**, 2254–2271.

DelSole, T., 2001: A simple model for transient eddy momentum fluxes in the upper troposphere. *J. Atmos. Sci.*, **58 (20)**, 3019–3035.

Edmon, H. J., B. J. Hoskins, and M. E. McIntyre, 1980: Eliassen-Palm cross sections for the troposphere. *J. Atmos. Sci.*, **37**, 2600–2616.

Haigh, J. D., M. Blackburn, and R. Day, 2005: The response of tropospheric circulation to perturbations in lower-stratospheric temperature. *J. Climate*, **18**, 3672–3685.

Held, I., 2005: The gap between simulation and understanding in climate modeling. *Bulletin of the American Meteorological Society*, **86**, 1609–1614.

Held, I. M., 1993: Large-scale dynamics and global warming. *Bulletin of the American Meteorological Society*, **74**, 228–242.

Held, I. M. and B. J. Hoskins, 1985: Large-scale eddies and the general circulation of the troposphere. *Advances in Geophysics.*, **28**, 3–31.

Held, I. M., R. L. Panetta, and R. T. Pierrehumbert, 1985: Stationary external Rossby waves in vertical shear. *J. Atmos. Sci.*, **42 (9)**, 865–883.

Held, I. M. and P. Phillips, 1987: Linear and nonlinear barotropic decay on the sphere. *J. Atmos. Sci.*, **44**, 200–207.

Held, I. M. and M. J. Suarez, 1994: A proposal for the intercomparison of the dynamical cores of atmospheric general circulation models. *Bull. Amer. Meteor. Soc.*, **75**, 1825–1830.

Hoskins, B. J. and D. J. Karoly, 1981: The steady linear response of a spherical atmosphere to thermal and orographic forcing. *J. Atmos. Sci.*, **38**, 1179–1196.

Hoskins, B. J., M. E. McIntyre, and A. W. Robertson, 1985: On the use and significance of isentropic potential vorticity maps. *Quart. J. Roy. Meteor. Soc.*, **111**, 877–946.

Kidston, J., S. M. Dean, J. A. Renwick, and G. K. Vallis, 2010: A robust increase in the eddy length scale in the simulation of future climates. *Geophys. Res. Lett.*, **37**, L03 806.

Kidston, J. and G. K. Vallis, 2010: Relationship between eddy-driven jet latitude and width. *Geophys. Res. Lett.*, **37**, L21 809.

Kidston, J. and G. K. Vallis, 2012: The relationship between the speed and the latitude of an eddy-driven jet in a stirred barotropic model. *J. Atmos. Sci.*, **69**, 3251–3263.

Kidston, J., G. K. Vallis, S. M. Dean, and J. A. Renwick, 2011: Can the increase in the eddy length scale under global warming cause the poleward shift of the jet streams? *J. Climate*, **24**, 3764–3780.

Lorenz, D. J., 2014a: Understanding mid-latitude jet variability and change using Rossby wave chromatography: Methodology. *submitted to J. Atmos. Sci.*

Lorenz, D. J., 2014b: Understanding mid-latitude jet variability and change using Rossby wave chromatography: Wave-mean flow interaction. *submitted to J. Atmos. Sci.*

Lorenz, D. J. and E. T. DeWeaver, 2007: Tropopause height and zonal wind response to global warming in the IPCC scenario integrations. *J. Geophys. Res.*, **112**, D10 119.

Lu, J., G. Chen, and D. M. W. Frierson, 2008: Response of the zonal mean atmospheric circulation to El Niño versus global warming. *J. Climate*, **21**, 5835–5851.

Manabe, S. and R. T. Wetherald, 1967: Thermal equilibrium of the atmosphere with a given distribution of relative humidity. *J. Atmos. Sci.*, **24**, 241–259.

Manabe, S. and R. T. Wetherald, 1980: On the distribution of climate change resulting from an increase in CO_2 content of the atmosphere. *J. Atmos. Sci.*, **37**, 99–118.

Pierrehumbert, R. T. and K. L. Swanson, 1995: Baroclinic instability. *Annual review of fluid mechanics*, **27**, 419–467.

Randel, W. J. and I. M. Held, 1991: Phase speed spectra of transient eddy fluxes and critical layer absorption. *J. Atmos. Sci.*, **48**, 688–697.

Rivière, G., 2011: A dynamical interpretation of the poleward shift of the jet streams in global warming scenarios. *J. Atmos. Sci.*, **68**, 1253–1272.

Robinson, W. A., 1997: Dissipation dependence of the jet latitude. *J. Climate*, **10**, 176–182.

Robinson, W. A., 2000: A baroclinic mechanism for the eddy feedback on the zonal index. *J. Atmos. Sci.*, **57**, 415–422.

Saravanan, R., 1993: Equatorial superrotation and maintenance of the general circulation in two-level models. *J. Atmos. Sci.*, **50 (9)**, 1211–1227.

Simmons, A. J. and B. J. Hoskins, 1978: The life cycles of some nonlinear baroclinic waves. *J. Atmos. Sci.*, **35**, 414–432.

Simpson, I. R., M. Blackburn, and J. D. Haigh, 2009: The role of eddies in driving the tropospheric response to stratospheric heating perturbations. *J. Atmos. Sci.*, **66 (5)**, 1347–1365.

Simpson, I. R., M. Blackburn, and J. D. Haigh, 2012: A mechanism for the effect of tropospheric jet structure on the annular mode-like response to stratospheric forcing. *J. Atmos. Sci.*, **69**, 2152–2170.

Simpson, I. R., M. Blackburn, J. D. Haigh, and S. N. Sparrow, 2010: The impact of the state of the troposphere on the response to stratospheric heating in a simplified GCM. *J. Climate*, **23**, 6166–6185.

Thorncroft, C. D., B. J. Hoskins, and M. E. McIntyre, 1993: Two paradigms of baroclinic-wave life-cycle behaviour. *Quart. J. Roy. Meteor. Soc.*, **119**, 17–55.

Vallis, G. K., E. P. Gerber, P. J. Kushner, and B. A. Cash, 2004: A mechanism and simple dynamical model of the North Atlantic Oscillation and annular modes. *J. Atmos. Sci.*, **61**, 264–280.

Williams, G. P., 2006: Circulation sensitivity to tropopause height. *J. Atmos. Sci.*, **63**, 1954–1961.

Wu, Y., R. Seager, T. A. Shaw, M. Ting, and N. Naik, 2013: Atmospheric circulation response to an instantaneous doubling of carbon dioxide. Part II: Atmospheric transient adjustment and its dynamics. *J. Climate*, **26 (3)**, 918–935.